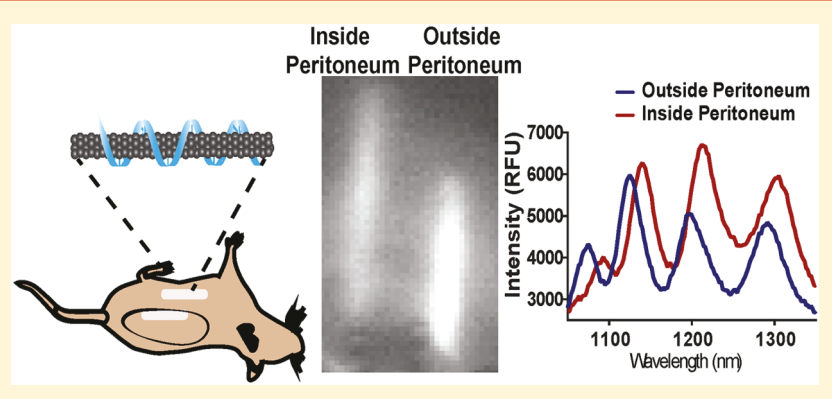
Exposure

Downloaded via MEMORIAL SLOAN-KETTERING CANCER CTR on January 17, 2020 at 19:59:42 (UTC). See https://pubs.acs.org/sharingguidelines for options on how to legitimately share published articles.

An in Vivo Nanosensor Measures Compartmental Doxorubicin

Jackson D. Harvey, †,‡,||© Ryan M. Williams, †,||© Kathryn M. Tully, †,‡ Hanan A. Baker, †,‡ Yosi Shamay, †,§ and Daniel A. Heller*,†,‡

Supporting Information



ABSTRACT: Preclinical measurements of drug exposure to specific organs and tissues is normally performed by destructive methods. Tissue-specific measurements are important, especially for drugs with intractable dose-limiting toxicities, such as doxorubicin-mediated cardiotoxicity. We developed a method to rapidly quantify doxorubicin exposure to tissues within living organisms using an implantable optical nanosensor that can be interrogated noninvasively following surgical implantation. The near-infrared fluorescence of single-walled carbon nanotubes functionalized with DNA was found to respond to doxorubicin via a large and uniform red-shift. We found this to be common to DNA-intercalating agents, including anthracycline compounds such as doxorubicin. Doxorubicin was measured in buffer and serum, intracellularly, and from single nanotubes on a surface. Doxorubicin adsorption to the DNA-suspended nanotubes did not displace DNA but bound irreversibly. We incorporated the nanosensors into an implantable membrane which allowed cumulative detection of doxorubicin exposure in vivo. On implanting the devices into different compartments, such as subcutaneously and within the peritoneal cavity, we achieved real-time, minimally invasive detection of doxorubicin injected into the peritoneal cavity, as well as compartment-specific measurements. We measured doxorubicin translocation across the peritoneal membrane in vivo. Robust, minimally invasive pharmacokinetic measurements in vivo suggest the suitability of this technology for preclinical drug discovery applications.

KEYWORDS: Pharmacology, toxicology, nanocarbons, biosensor, photoluminescence

Real-time, transient monitoring of drug pharmacokinetics in preclinical models and patients remains a hurdle to therapeutic efficacy and toxicological analyses. Tissue-specific measurements of drug exposure are important for understanding drug toxicities and therapeutic windows, as is drug penetration across delivery barriers. For drugs with unmanageable dose-limiting toxicities, it is especially necessary to understand fluctuations in exposure and lifetime total exposure. The measurement of preclinical drug exposure to specific organs and tissues is normally measured by destructive methods, requiring dissection. Quantification of drug biodistribution normally requires end point analysis and euthanization of multiple animals for each time point. Such pharmacokinetic analyses in preclinical and clinical development would benefit from a rapid, facile measurement of drug concentrations and total exposure in multiple body compartments.

An important class of cancer drugs that exhibit severe doselimiting toxicities are the anthracyclines, which include daunorubicin, doxorubicin, epirubicin, idarubicin, and valrubicin. Doxorubicin in particular has become one of the most widely used chemotherapy drugs and is used to treat breast cancer, acute lymphoblastic leukemia, bladder cancer, Ewing sarcoma, Hodgkin lymphoma, non-Hodgkin lymphoma, osteosarcoma, recurrent small cell lung cancer, and soft tissue

Received: March 6, 2019 Revised: June 10, 2019 Published: June 18, 2019

^{*}Memorial Sloan Kettering Cancer Center, New York, New York 10065, United States

^{*}Weill Cornell Medicine, New York, New York 10065, United States

[§]Technion—Israel Institute of Technology, Haifa 3200003, Israel

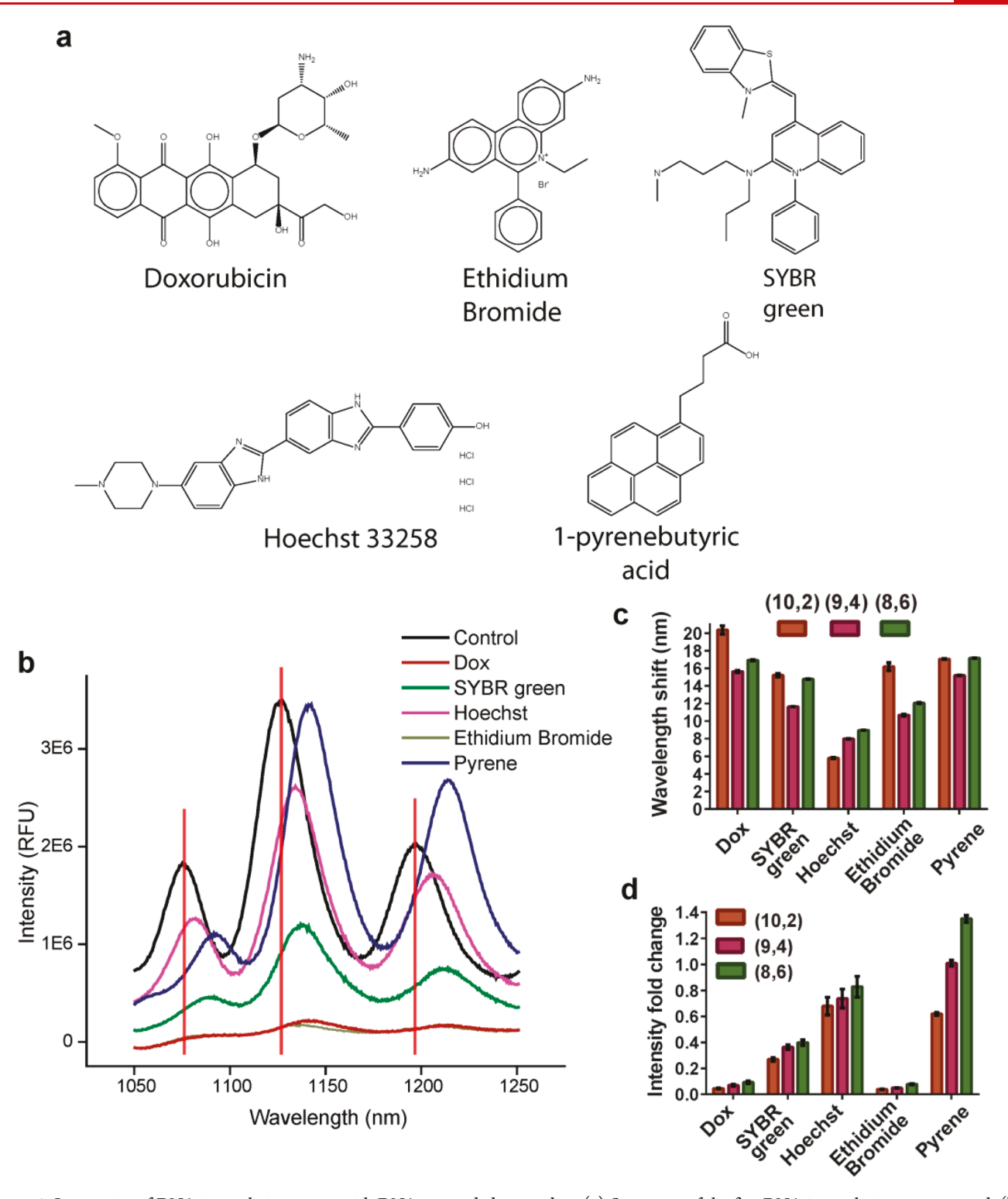


Figure 1. Interaction of DNA-intercalating agents with DNA-suspended nanotubes. (a) Structures of the five DNA-intercalating agents tested. (b) Representative spectra of DNA-suspended nanotubes after addition of 1 μ M each of the indicated compound. Red horizontal lines represent the center wavelength for control nanotubes (exposed to no compound) of the (10,2), (9,4), and (8,6) chiralities. (c) Wavelength shift relative to a buffer-treated control for three chiralities after addition of 1 μ M of the indicated compound. Data are presented as mean \pm SD of technical triplicates. (d) Corresponding intensity fold change relative to buffer-treated control for three chiralities after addition of 1 μ M of the indicated compound. Data are presented as mean \pm SD of technical triplicates.

sarcomas.² Despite the broad efficacy of doxorubicin, its administration must be closely monitored due to dose-limiting cardiotoxicity, which is cumulative and irreversible, limiting both acute and lifetime dosing of the drug. On the basis of retrospective analyses of clinical events, the incidence of

cardiotoxicity is about 7.5% at a lifetime dose of 550 mg/m $^{23-5}$ which has become the recommended upper limit. This limit is pragmatic from an epidemiological perspective, as it is not possible to predict patient-specific lifetime dose limits. Doxorubicin is typically administered intravenously (IV) and

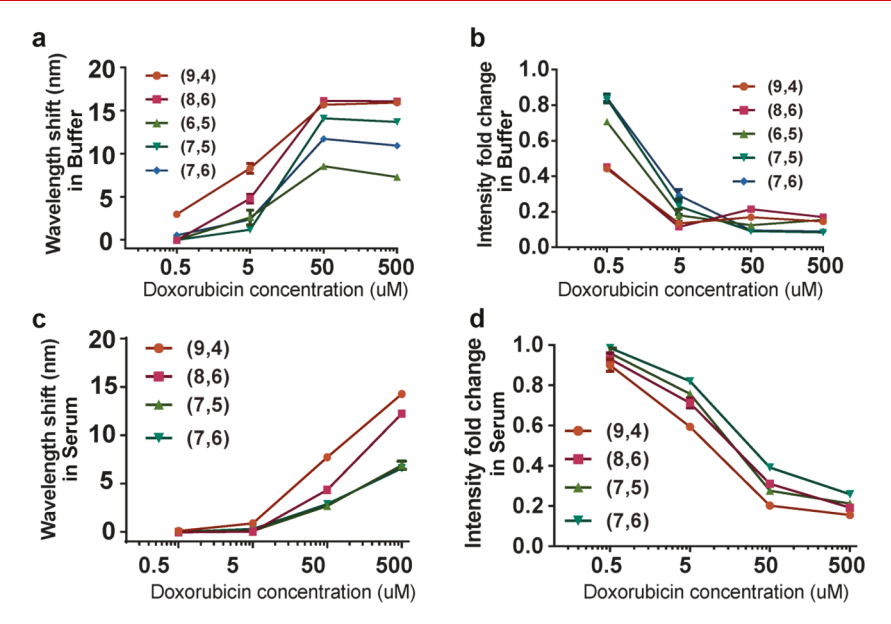


Figure 2. Sensitivity and kinetics of the nanosensor response to doxorubicin. (a) Change in emission band center wavelength of 5 nanotube chiralities as a function of doxorubicin concentration in buffer conditions. (b) Intensity change relative to buffer-treated control for 5 nanotube chiralities as a function of doxorubicin concentration in buffer conditions. (c) Change in band center wavelength of 5 nanotube chiralities as a function of doxorubicin concentration in whole serum. (d) Intensity change relative to serum control for 5 nanotube chiralities as a function of doxorubicin concentration in whole serum. Error bars represent standard deviation of technical triplicates.

is also administered at high doses into the peritoneum in certain conditions, such as metastatic ovarian cancer. ^{6,7} For both traditional IV administration and peritoneal administration, tissue-specific monitoring could potentially allow the assessment of drug distribution in particular anatomic sites in real-time. A cumulative sensor near or within cardiac tissue could also provide precise information on patient-specific exposure to doxorubicin and eventually enable better control of lifetime exposure to doxorubicin and prevention of cardiomyopathy.

Anthracyclines and several other important compounds interact with DNA via intercalation. DNA intercalation is a noncovalent interaction driven by hydrophobic and π - π interactions between a planar, aromatic polycyclic compound that is approximately the size of two DNA bases.^{8,5} Intercalation often distorts the DNA¹⁰ to prevent replication or other essential cell functions, 11 which is therapeutically useful for halting cell division in cancer cells¹² but can also be highly toxic to normal dividing cells. 13 DNA-intercalating agents have additionally found widespread use in molecular biology to visualize DNA, such as ethidium bromide¹⁴ and others. 15,16 Some pollutants are also recognized to be intercalating agents with carcinogenic potential, such as polycyclic aromatic hydrocarbons (PAHs).¹⁷ Rapid optical detection of PAHs could be beneficial for environmental monitoring 18,19 or other toxicology applications.

Single-walled carbon nanotubes (SWCNTs) are nanomaterials with unique DNA-binding properties that have been used to develop in situ optical and electronic sensors. SWCNTs are cylinders composed entirely of sp² hybridized carbon, essentially consisting of graphene rolled into a cylinder with a diameter between about 0.8 and 1.2 nm. Single-walled nanotubes can be noncovalently suspended by single-stranded nucleic acids which bind to carbon nanotubes via π - π stacking interactions between the nucleobases and the graphitic/aromatic nanotube surface. Flexibility in the single-stranded DNA backbone enables wrapping around the nanotube surface

so that multiple bases can bind, providing a high-avidity interaction. 21,22 The negatively charged phosphate backbone serves to prevent reaggregation through electrostatic repulsion, 23 making single-stranded DNA an effective dispersant for preparing colloidal solutions of carbon nanotubes. SWCNTs emit highly photostable band gap photoluminescence (fluorescence) 24,25 in the near-infrared range, which is penetrant to living tissues. 26 The single-walled carbon nanotube emission is highly sensitive to their local dielectric environment. 27,28 DNA-encapsulated nanotubes are similarly environmentally responsive and have been applied in the detection of several analytes such as lipids, alkylating chemotherapeutic drugs, cell-surface and soluble proteins, and microRNA, among others. 29–35 DNA-SWCNT sensors have been employed *in vivo* for the detection of analytes including reactive oxygen species, microRNA, and protein biomarkers for cancer. 33,36,37

Certain DNA intercalators exhibit a strong affinity for the carbon nanotube surface³⁸ and can be used to noncovalently solubilize them.³⁹ Doxorubicin has been shown to bind carbon nanotubes that have been suspended with PEGylated lipids,⁴⁰ which were used as a vector for drug delivery.⁴¹ We previously found that the interaction of DNA-suspended nanotubes and amphiphilic surfactants can be discerned via changes in carbon nanotube photoluminescence, and we found that amphiphiles bind to the remaining free space on the nanotube surface.³³ Given the strong affinity of DNA intercalators such as polycyclic aromatic hydrocarbons and doxorubicin for carbon nanotubes, we surmised that carbon nanotubes may be used to monitor these agents in biological environments, including *in vivo*, via the nanotube emission response.

Herein, we investigated the impact of DNA-intercalating agents on the optical properties of carbon nanotubes and their *in vivo* application. We found that the binding of DNA intercalators to the carbon nanotube surface resulted in redshifting of the emission and excitation wavelengths of carbon nanotube photoluminescence, likely due to charge carrier screening. Doxorubicin was found to elicit dose-dependent

red-shifting and quenching of ssDNA-suspended carbon nanotubes in both buffer and serum conditions with rapid kinetics. In exploring the mechanism, we found that the suspending DNA was not displaced, and approximately 180 molecules of doxorubicin irreversibly bound to a DNAwrapped nanotube of average length (166 nm). We also found that single nanotube complexes could detect doxorubicin in both buffer and serum conditions, largely recapitulating the average bulk response. Three modalities of implantable devices were tested in vitro; two hydrogels, agarose and alginate, and a heat-sealable semipermeable membrane. Using the semipermeable membrane-based device, we found that sensing resulted in a cumulative response. Surgical implantation into the peritoneal cavity of a mouse allowed for rapid, minimally invasive optical detection of injected doxorubicin. Finally, we implanted two devices in sites separated by the peritoneal membrane. After administering doxorubicin, we found an anatomically distinct response denoting that the drug did not appreciably pass through this thin layer of tissue.

Results and Discussion. We interrogated DNA-suspended carbon nanotubes with a panel of known DNAintercalating agents, to assess the response on nanotube photoluminescence. Three of the compounds, ethidium bromide, SYBR green, and Hoechst 33258, are used to measure DNA content by fluorescent changes after intercalation. Doxorubicin, a chemotherapy drug, is an effective agent against rapidly dividing cells due in part to its affinity for DNA. A conjugate of polyethylene glycol (PEG) and pyrene (pyrene-PEG) was synthesized by reacting amine-terminated polyethylene glycol (PEG, 1000 MW) with NHS-activated 1pyrenebutyric acid (see methods in the Supporting Information) (Figure 1a). Each agent elicited red-shifting behavior from the carbon nanotube emission (Figure 1b,c). The emission intensity for most agents was reduced to varying degrees, with 1 μ M doxorubicin and ethidium bromide producing the greatest reductions (Figure 1b,d). This concentration is approximately equal to potential physiological concentrations, as prior work has shown patient blood doxorubicin levels ranging up to 0.92 μ M. Because of the potential clinical utility of an optical sensor for doxorubicin, we further characterized this interaction.

We assessed the quantitative behavior of the DNAnanotube hybrids in response to doxorubicin. A dilution experiment found that most nanotube chiralities exhibited dose-dependent red-shifting at doxorubicin concentrations between 500 nM and 50 uM after a 4 h incubation (Figure 2a). In these experiments, the limit of detection of the sensor was 5 μ M doxorubicin for all chiralities except for the (9,4), for which it was 500 nm. The nanotube emission quenched 60-80% upon incubation with 5 μ M doxorubicin and even 20– 50% at 0.5 μ M doxorubicin (Figure 2b). All chiralities were sensitive to as low as 500 nm doxorubicin using intensity-based measurements. The kinetics of the nanotube emission response were measured upon introducing doxorubicin. The wavelength shifting and intensity quenching responses were rapid, with a large amount of the observed sensor response occurring between sample addition and the first measurement obtained on our instrumentation (Figure S1).

We next investigated the possibility of quantitative sensing of doxorubicin in complex biological solutions such as serum. We previously reported that serum nonspecifically red-shifts carbon nanotube emission due to electrostatic interactions with serum proteins.³³ We repeated our earlier dose–response experiment in serum. We observed dose-dependent redshifting (Figure 2c) and intensity quenching (Figure 2d; Figure S2), with sensitivity reduced by approximately 1 order of magnitude as compared to buffer-only conditions: 50 μ M for all chiralities but (9,4) (5 μ M) by wavelength shift and 5 μ M for all chiralities by intensity change. One explanation for this change in sensitivity may be that doxorubicin is known to bind to serum proteins,⁴³ which may have lowered the availability of the free drug to bind to the sensor.

Mechanistic studies were conducted to understand the nature of the doxorubicin-induced optical response of the nanotubes. We first investigated whether the aggregation and fluorescence quenching of DNA-suspended sensor complexes were due to aggregation with metallic nanotubes (see text in the Supporting Information). However, experiments with SWCNT preparations lacking metallic nanotubes determined that aggregation did occur, and this was likely not to be the cause of quenching (Figure S3). We then assessed whether doxorubicin displaced the DNA from the nanotube surface by competing for interaction with the adsorbing nucleotide bases (see text in the Supporting Information). However, displacement experiments of fluorescently labeled DNA-SWCNT complexes revealed that the wrapped DNA is not displaced by doxorubicin (Figure S4).

We attempted to measure the quantity of doxorubicin that bound to DNA-suspended nanotubes. A known mass of $(GT)_{15}$ -suspended nanotubes was added to 500 μ M doxorubicin, and an equal volume of buffer was added to a control. After incubation, the samples were centrifuged to pellet the aggregated nanotubes (Figure S5a), and a sample of the supernatant was assayed for doxorubicin using absorbance spectra (Figure S5b). The difference in absorbance was compared to a doxorubicin standard curve (Figure S5c) and used to estimate the mass of doxorubicin lost from solution due to binding the nanotubes. From these data, we estimate that 1 μ g of (GT)₁₅-suspended nanotubes bound to 0.95 μ g of doxorubicin. This is less than in previous work of doxorubicin loading on phospholipid-PEG-suspended nanotubes, which reported a 4:1 ratio of doxorubicin to carbon nanotube by mass.⁴⁰ The authors estimated the phospholipid-PEG coating to cover only 10% of the nanotube surface, which may explain the difference we observed with a DNA coating. We next attempted to wash away the bound doxorubicin by pelleting the sample, aspirating the supernatant, and adding 100 μ L of buffer and vortexing. This was performed three times, with the supernatant extracted for absorbance measurements after each wash (Figure S6a). The first wash released some doxorubicin from the nanotubes, giving the supernatant a red hue. The following washes did not change the supernatant color, but the nanotube pellet continued to appear red. On the basis of a comparison of the absorbance of the supernatant from each wash (Figure S6b) to the standard curve, we calculated that about 0.35 μ g of doxorubicin was removed from the nanotube surface by washing. We conclude that 0.6 μ g of doxorubicin bound to 1 μ g of (GT)₁₅-suspended nanotubes strongly enough to resist desorption from pelleting and washing. The average length of carbon nanotubes in our sample is 166 nm. 44 We estimate that the average mass of a nanotube of this length (using the (6,5) species) is 3×10^{-19} g, based on previous calculations. 45 Thus, for one nanotube, we calculate that approximately 180 molecules of doxorubicin bound strongly. The emission spectra from the nanotubes were acquired after

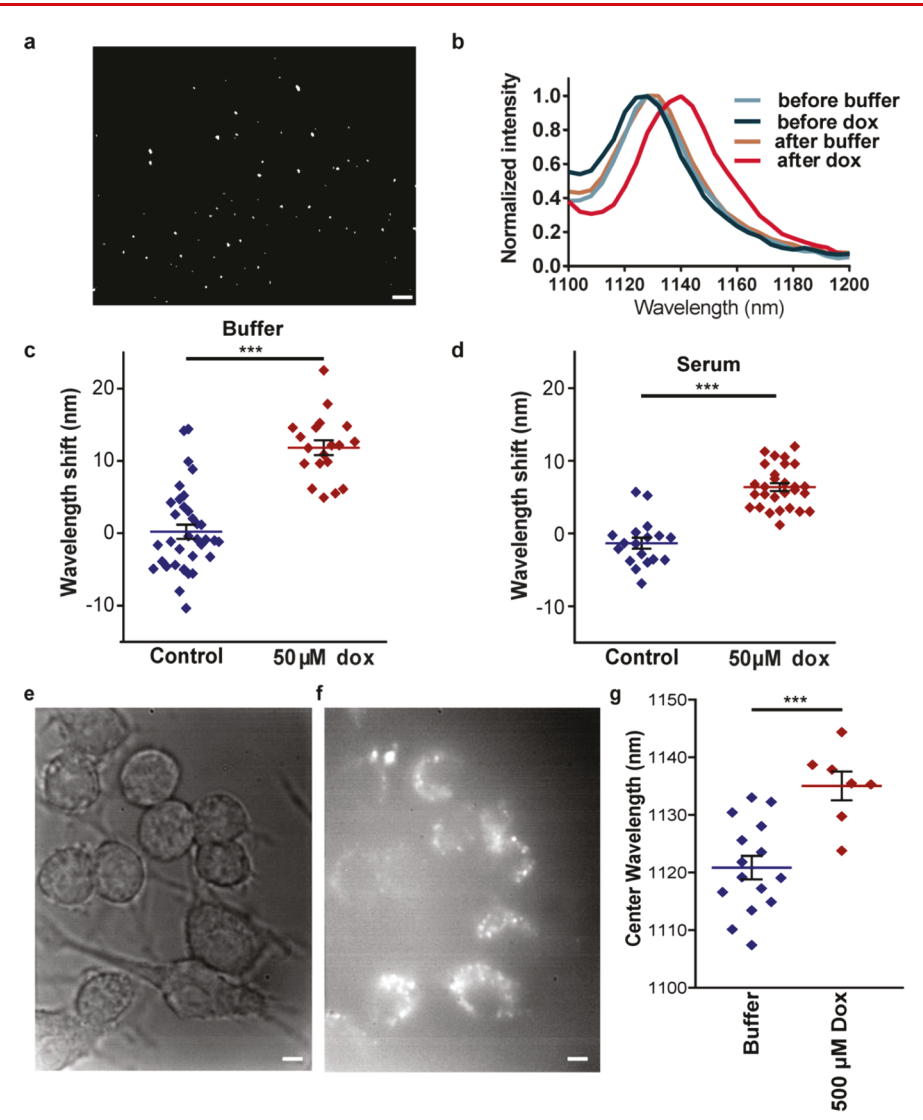


Figure 3. Single-nanotube response to doxorubicin. (a) Representative near-infrared photoluminescence image of carbon nanotubes on the surface of a lysine-coated glass bottom plate in buffer. Scale bar = 5 μ M. (b) Composite spectrum of all single nanotube spectra upon interrogation with buffer (control) or 50 μ M Dox. (c) Wavelength shifting response of single nanotubes in buffer treated with 50 μ M doxorubicin or buffer only. Buffer only n = 36; doxorubicin n = 19; $p = 3.0 \times 10^{-10}$; unpaired two-tailed t test. Each point represents a single nanotube. Center line represents mean. Error bars represent SEM. (d) Wavelength shifting response of single nanotubes in whole serum treated with buffer or 50 μ M doxorubicin. Buffer n = 18; doxorubicin n = 28; $p = 9.5 \times 10^{-11}$; unpaired two-tailed t test. Each point represents a single nanotube. Center line represents mean. Error bars represent SEM. (e) White light image of macrophages on a glass surface at $1000 \times magnification$. Scale bar = 5 μ M. (f) Broadband near-infrared emission under 730 nm excitation corresponding to the region of interest depicted in panel e. Scale bar = 5 μ M. (g) Center wavelength of all nanotubes within individual cells treated with either buffer or 500 μ M doxorubicin. Each bar is mean \pm SEM; n = 15 cells for buffer, n = 7 cells for dox; $p = 5.5 \times 10^{-4}$; unpaired two-tailed t test. Each point represents a single cell. Center line represents mean. Error bars represent SEM.

treatment with buffer, 500 μ M Dox, or 500 μ M doxorubicin followed by three washes, to assess the impact of washing on the nanotube optical response to doxorubicin (Figure S6c). We observed that the emission spectrum was largely unaltered by washing as compared to the sample containing 500 μ M doxorubicin without pelleting and washing (Figure S6d). We conclude that 0.6 μ g of doxorubicin bound nearly irreversibly to 1 μ g of (GT)₁₅-suspended nanotubes, leading to the observed nanotube emission changes. Additional doxorubicin that was less strongly bound did not appear to contribute further to the optical changes, as its removal had little impact on the nanotube emission.

Single-nanotube responses to doxorubicin were assessed in buffer conditions and in serum. DNA-suspended nanotubes were incubated on a lysine-coated glass bottom plate for 10 min before washing and replacing the buffer. Single nanotubes were apparent on the surface upon imaging using a fluorescence microscope with 730 nm excitation and broadband image acquisition (Figure 3a). Spectra of individual (9,4) nanotubes were acquired via near-infrared hyperspectral imaging 46 (Figure 3b). After 10 min of incubation with buffer, as a control, or concentrated doxorubicin to a final concentration of 50 μ M, the spectra were acquired again, and the emission wavelength shift of each individual nanotube was calculated. Treatment with doxorubicin produced an overall wavelength red-shift of 11.6 nm \pm 1.5 nm (Figure 3c). The signal change of the averaged spectrum of the single nanotubes (11.6 nm) approached that of the bulk spectrum from the suspension material (15.6 nm). We next measured the response of single (9,4) nanotubes in whole serum upon

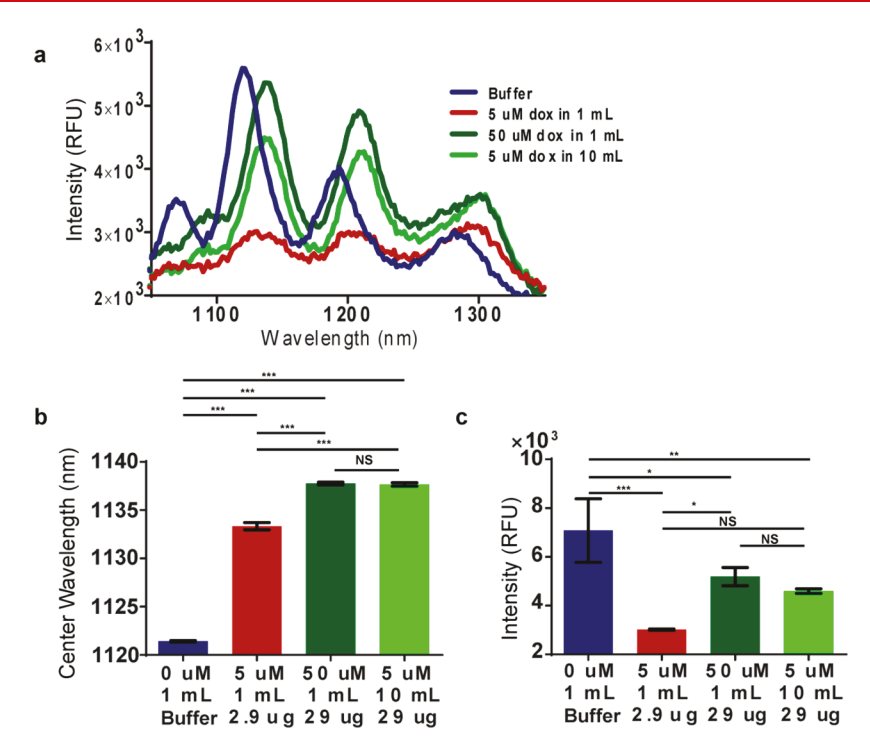


Figure 4. Detection of doxorubicin is cumulative. (a) Representative emission spectra of DNA-suspended nanotubes in an implantable membrane device after overnight incubation in 1 mL of buffer, 1 mL of 5 μM doxorubicin, 1 mL of 50 μM doxorubicin, or 10 mL of 5 μM doxorubicin. (b) (9,4) center wavelength from spectra in panel a with doxorubicin concentration, volume, and total mass of doxorubicin listed below. N = 3; mean \pm SD; one-way ANOVA with Tukey's multiple comparisons test; bar 1-2*** = $p = 5 \times 10^{-10}$; bar 1-3*** = $p = 5 \times 10^{-10}$; bar 1-4*** = $p = 5 \times 10^{-10}$; bar 1-4*** = $p = 7.6 \times 10^{-9}$; bar 1-4*** = $p = 9.3 \times 10^{-9}$; bar 1-4 NS = p = 0.96. (c) Intensity corresponding to the data in panels a and b. N = 3; mean \pm SD; one-way ANOVA with Tukey's multiple comparisons test; bar 1-2*** = $p = 3.8 \times 10^{-4}$; bar 1-3* = p = 0.037; bar 1-4** = p = 0.0089; bar 2-3* = p = 0.019; bar 2-4 NS = p = 0.08; bar 3-4 NS = p = 0.72. No significant difference in intensity between incubation in 1 mL of 50 μM doxorubicin or 10 mL of 5 μM doxorubicin. Error bars represent standard deviation of three measurements.

introducing doxorubicin. The average magnitude of redshifting was 7.7 ± 0.9 nm (Figure 3d). The averaged shift from single nanotubes of 7.7 nm closely recapitulated the bulk measurement.

Because the nanosensor responded to doxorubicin in a complex protein environment, we tested whether doxorubicin could be detected within live cells. (GT)₁₅-suspended nanotubes were incubated with the RAW 264.7 murine macrophage cell line overnight and washed three times to remove cell surface-adsorbed nanotubes.³⁰ White light images showed normal cell morphology (Figure 3e), and broadband near-infrared images revealed punctate spots of nanotube-filled vesicles inside most of the cells as expected from prior works (Figure 3f). 30,47,48 Three cohorts of cells were treated with 500 μ M doxorubicin or buffer, as a control, and incubated for 1 h, after which the nanotube emission was measured via hyperspectral microscopy focusing on the (9,4) nanotube chirality. We confirmed that the nanotube center wavelength was not dependent upon the total fluorescence intensity within each cell (Figure S7). Treatment with 500 µM doxorubicin elicited an average per-cell red-shift of approximately 14 nm (Figure 3g). DNA-nanotube complexes are known to internalize via endocytosis or phagocytosis,⁴⁹ and the nanotubes remain localized in vesicles within the cell. Cell viability is unaffected by this treatment with nanotubes. 50,51 The nanotube response to doxorubicin is almost identical to that which was found in solution-based serum measurements above (Figure 2c).

To construct an implantable sensor for doxorubicin, three different materials were tested. We first encapsulated DNA-

suspended nanotubes in agarose gel, known to carry nanotube complexes without diminishing their photoluminescence. 52 The sensor response to doxorubicin within the gels in vitro closely resembled that of unencapsulated nanotube complexes, and the kinetics were unaffected by gel encapsulation, with maximal red-shifting and intensity quenching by 10 min (Figure S8a). To examine reversibility, the doxorubicin-treated nanotube-impregnated agarose gel (about 20 μ L volume) was dialyzed in 50 mL of deionized (DI) water with three changes, where the last change was allowed to proceed overnight. The nanotube emission red-shift was not reversed by the dialysis, consistent with the inability to wash away doxorubicin in previous experiments. Another hydrogel, alginate, was tested due to its ease of use and precedent for use in vivo with suspended nanotubes for sensing applications.³⁶ Again, we observed red-shifting and quenching in response to doxorubicin, making this hydrogel a potential implantation material (Figure S8b). Lastly, we tested a porous membrane wherein the nanotube solution was heat-sealed inside, as we have previously reported. 33,37 An in vitro dose-response assessment produced a surprising pattern, where concentrations above 5 μM doxorubicin resulted in nanotube red-shifting, but the intensity did not quench to the degree seen in the other materials. Certain nanotube chiralities produced even brighter intensities than the baseline intensity, before introduction of doxorubicin (Figure S8c). When the DNA-nanotubeencapsulated membranes were tested in vitro in whole serum, we noted a similar phenomenon, but where maximal quenching occurred at 50 μ M of doxorubicin rather than 5

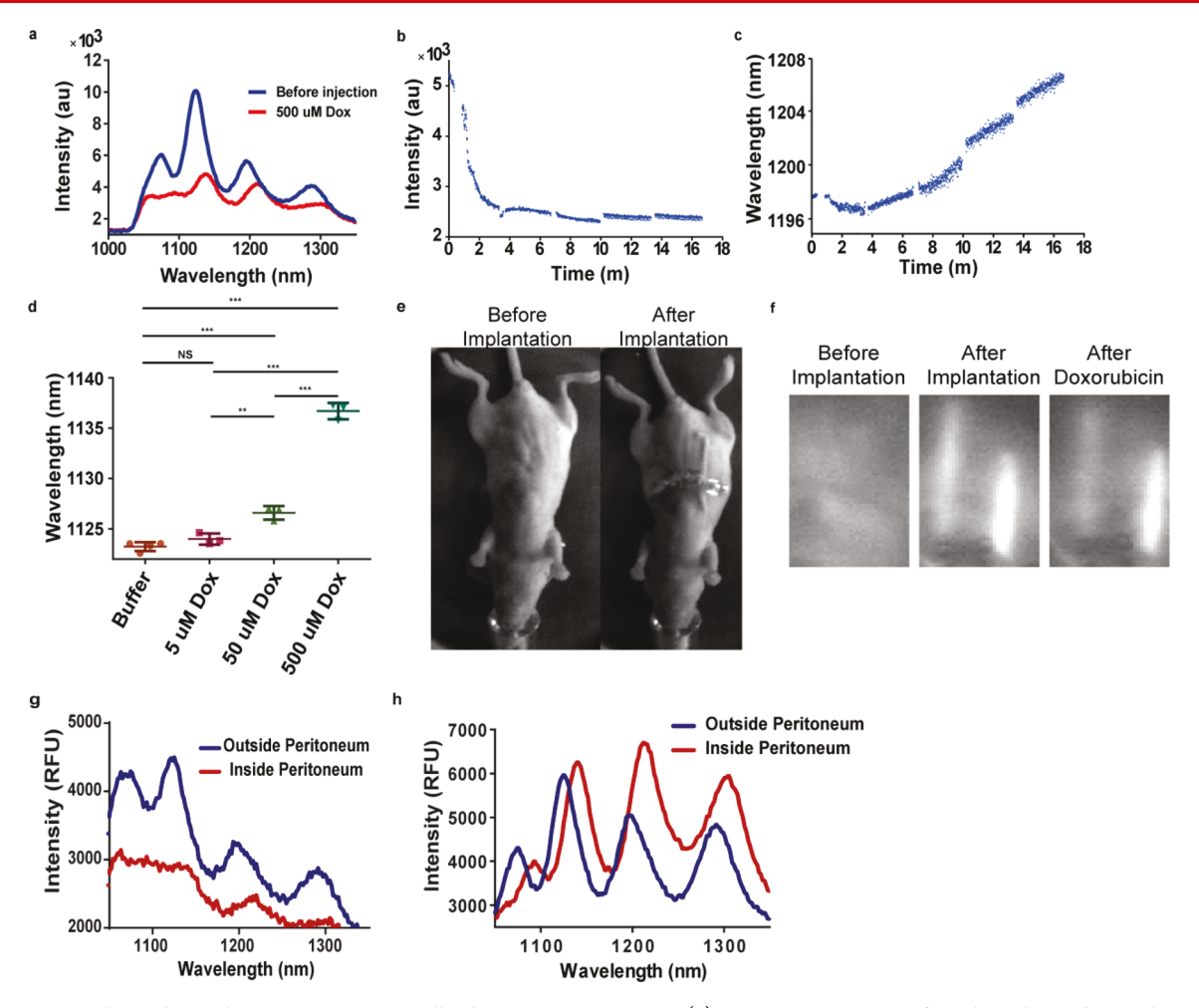


Figure 5. *In vivo* doxorubicin detection in anatomically distinct compartments. (a) Emission spectrum of implanted membrane device before injection of doxorubicin and 30 min after intraperitoneal injection of 1 μ L of μ M doxorubicin. (b) Intensity of implanted nanotube device measured for the (8,6) in real-time after intraperitoneal injection of 1 mL of doxorubicin at time 0 min. (c) Center wavelength of the (8,6) nanotube device measured in real-time after intraperitoneal injection. Kinetics data were taken every 0.5 s for the duration of the experiment. Gaps in data are from periodic monitoring of the mouse. (d) Center wavelength of the (9,4) nanotube from implanted membrane devices after injection with 1 mL of buffer, 5 μ M Dox, 50 μ M Dox, or 500 μ M Dox. N = 3-4; mean \pm SD; one-way ANOVA with Tukey's multiple comparisons test; buffer vs 5 μ M Dox NS = p = 0.43; buffer vs 50 μ M Dox *** = $p = 2.8 \times 10^{-4}$; buffer vs 500 μ M Dox *** = $p = 2.4 \times 10^{-9}$; 5 μ M Dox vs 500 μ M Dox *** = p = 0.0029; 5 μ M Dox vs 500 μ M Dox *** = $p = 4.7 \times 10^{-9}$; 50 μ M Dox vs 500 μ M Dox *** = $p = 4.2 \times 10^{-8}$. (e) Image of the mouse before surgery (left) and after implantation of sensors in peritoneum and under skin (right). (f) Broadband near-infrared emission from a mouse before sensor implantation (left), after implantation (center), and after injection of 500 μ M doxorubicin. The device on the left of each image was implanted in the peritoneum) and inside the peritoneum (red) as measured with probe apparatus. (h) Emission spectra of the device under the skin (blue, outside peritoneum) and inside the peritoneum (red) taken *ex vivo* after the experiment.

 μ M, consistent with a reduction in serum-based sensitivity (Figure S8d).

To better understand the restoration of intensity with higher concentrations of doxorubicin using the dialysis membrane, more concentrations were tested around and below 5 μ M. We observed that the nanotube emission wavelength did not shift at concentrations less than 1 μ M. However, at lower concentrations where a red-shift could be detected, the intensity quenched. Beyond about 5 μ M, the intensity restored to levels comparable to untreated controls (Figure S9a). While analyzing the wavelength shift of carbon nanotubes has several advantages as a sensor output for an implantable sensor, it is also possible to make use of ratiometric intensity changes to control for factors that could change absolute intensity, such as heterogeneity of emission absorbance and scattering through different tissue types. Thus, we measured the intensity ratio of

two nanotubes, the (9,4) and the (8,7), to test if ratiometric quenching could be measured in concentration regimes below 5 μ M. Indeed, we found that ratiometric sensing could improve our threshold of detection to between 50 and 500 nM (Figure S9b).

We assessed the possibility that the implantable nanosensor may detect doxorubicin in a cumulative manner. We hypothesized that the response of the implantable device to long-term incubation in a low concentration of doxorubicin in a large volume would be equivalent to incubation with a higher concentration in a small volume, at equivalent total drug masses. We prepared the nanotube-loaded membrane implantable devices and incubated the implants in 10 mL of 5 μ M doxorubicin and in 1 mL of 50 μ M overnight; in both cases the total mass of doxorubicin was 29 μ g. We also incubated overnight in 1 mL of buffer and 1 mL of 5 μ M

doxorubicin (2.9 μ g) to serve as controls. The controls behaved as expected, where 5 μ M doxorubicin treatment induced red-shifting and maximal quenching while 50 μ M doxorubicin further red-shifted the nanotubes and restored intensity (Figure 4a). In the experimental group, 5 μ M doxorubicin in 1 mL again induced red-shifting and maximal quenching. Notably, the 5 μ M doxorubicin in 10 mL produced a spectrum that was nearly identical to that of incubation in 1 mL of 50 μ M doxorubicin (Figure 4a). We assessed the center wavelength (Figure 4b) and intensity (Figure 4c) for the (9,4) nanotube and found that the values were not statistically different.

We assessed the function of the nanosensor implant response to doxorubicin *in vivo*. We surgically placed the nanotube-loaded membrane-based implant device into the peritoneal cavity of live mice. 33,37 After allowing the animals to awaken and become ambulatory for 1 h, they were again anesthetized with isoflurane. Fluorescence measurements of the implanted carbon nanotubes were taken through the skin with a custom-built laser probe apparatus consisting of a 730 nm laser and spectrometer coupled to an InGaAs array detector. 33,37 Following the measurement, 1 mL of 500 μ M doxorubicin was administered intraperitoneally, and the mice were again allowed to awaken and become ambulatory. After 30 m, the mice were again anesthetized, and nanotube implant fluorescence was measured. Injected doxorubicin produced the expected red-shift and intensity quenching (Figure 5a).

We measured the implant continuously to assess the kinetics of doxorubicin binding immediately after injection. We repeated the previous implantation and doxorubicin administration experiment while monitoring the (8,6) nanotube continuously, both before and after doxorubicin injection, with 0.5 s data acquisitions. Initial quenching was observed (Figure 5b), followed by red-shifting (Figure 5c) at approximately 4 min. The mouse was periodically monitored (gaps in data) for any experimentally induced damage (e.g., skin damage, signs of distress), but none was found.

We next assessed the threshold of detection *in vivo*. We surgically implanted the nanotube sensor device into mice and injected either buffer, 5 μ M doxorubicin, 50 μ M doxorubicin, or 500 μ M doxorubicin intraperitoneally. We found significant red-shifting at both the μ M and 500 μ M doxorubicin concentrations while monitoring the (9,4) nanotube chirality, but not for 5 μ M (Figure 5d). We found similar shifting upon examination of the (8,6) chirality (Figure S10a), and an examination of the implantable devices *ex vivo* corroborated the *in vivo* response (Figure S10b,c). Detection of 50 μ M doxorubicin, but not 5 μ M doxorubicin, was consistent with the dose response data taken in whole serum.

Finally, we investigated whether implanted carbon nanotube sensor devices could be used to obtain anatomic compartment-specific measurements of doxorubicin. We surgically implanted two carbon nanotube devices into the peritoneal area separated by the peritoneum. This membrane defines the peritoneal cavity and separates it from the skin. One device was placed in the peritoneal cavity, while the other device was implanted between the skin and the peritoneum. Imaging using a custom-built whole-animal near-infrared preclinical hyperspectral imager was used to assess implant placement. Two white light images show the mouse before and after surgery, with one of the implantable devices visible beneath the skin (Figure 5e). Broadband near-infrared imaging under 730 nm illumination shows the nanotube emission from the two implanted devices.

The suture was also apparent in the near-infrared image due to slight autofluorescence of the suture material. Doxorubicin was injected intraperitoneally, and intensity of the nanotube fluorescence from the implanted devices was monitored (Figure 5f). Broadband imaging showed quenching of the device in the peritoneal cavity but not of the device under the skin (Figure 5f). Whole-animal hyperspectral data were then collected (Figure S11a). The emission response of the implant under the skin showed clear spectral similarities (Figure S11b), but the emission intensity was too low with respect to the background to discern changes in the emission wavelength of the peritoneal implant (Figure S11c). The mouse was then interrogated using the fiber optic probe-linked near-infrared spectrometer, where each of the devices was measured in vivo. Compared to the device implanted outside the peritoneum, the device inside red-shifted and quenched to a large degree (Figure 5g). Measurement of the devices ex vivo confirmed the red-shift observed in vivo (Figure 5h). The difference in the responses of the two sensors suggests that doxorubicin was largely restricted to the inside of the peritoneum for the course of this experiment.

The ability to quantitatively detect doxorubicin and related compounds *in vivo* could help address the issue of dose-monitoring for cumulative toxicity in patients by incorporating DNA-suspended nanotubes into an implantable device. The sensor responded via a red-shift, allowing quantitative measurements. The nanotube emission also responded to doxorubicin via quenching, which we ascribe to the electron-withdrawing character of doxorubicin creating nonradiative decay sites or electron dispersion on the nanotube sidewall. ^{53,54} This is supported by the partial intensity restoration by the reducing agent Trolox.

The optical response of the nanotube to doxorubicin was quite robust, even in the complex environment of whole serum, within live cells, and in vivo. The doxorubicin-induced redshifting did not reverse upon attempts to remove doxorubicin. Although potentially detrimental to certain types of measurements, cumulative sensing behavior is particularly useful for human clinical applications, as the toxicity of doxorubicin to patients is cumulative and irreversible. We envision the utility of a sensing device that could be implanted via a minimally invasive procedure. An implantable sensor could also be useful for doxorubicin as part of hyperthermic intraperitoneal chemotherapy (HIPEC) procedures, where site-specific measurement of doxorubicin can take place in live animals or patients. 55 This could help provide more precise therapy by accounting for patient-to-patient variation in doxorubicin distribution. In experimental model systems, it may also be possible to use this sensor to aid with pharmacokinetics studies by studying doxorubicin accessibility in live organisms. This may be especially helpful in understanding cancer resistance to doxorubicin as cell intrinsic processes or extrinsic processes in the context of the live animal.

Methods. Suspension of Carbon Nanotubes. For DNA suspensions, single-walled carbon nanotubes produced by the HiPCO process (Unidym, Sunnyvale, CA) were mixed with DNA oligonucleotides (IDT DNA, Coralville, IA) at a 2:1 mass ratio (DNA:SWCNT) in 1 mL of saline-sodium citrate (SSC) buffer and ultrasonicated for 30 min at 40% amplitude (Sonics & Materials, Inc.). For sodium deoxycholate (SDC) suspensions, 1 mg of HiPCO nanotubes was similarly sonicated in 2 wt %/vol SDC prepared in water. Following ultrasonication, the dispersions were ultracentrifuged (Sorvall

Discovery 90SE) for 30 min at 280 000g. To remove free DNA, 100 kDa Amicon centrifuge filters (Millipore) were used. The DNA–nanotube complexes were resuspended in saline-sodium citrate buffer (G Biosciences, St. Louis, MO). The top 80% of the supernatant was collected. Absorbance spectra for all dispersions were acquired using a UV/vis/NIR spectrophotometer (Jasco V-670, Tokyo, Japan). The concentration was calculated using the extinction coefficient $Abs_{910} = 0.025 54 \text{ L/(mg cm}^{146})$.

The DNA sequences used for suspension were as follows:

- (1) GTGTGTGTGTGTGTGTGTGTGTGTGTTGT-TCAGTTTTGCATAGATTTGCACA;
- (2) GTGTGTGTGTGTGTGTGTGTGTGTGT (denoted (GT)₁₅);
- (4) CTTCCCTTC-Cy5.

All were purchased from IDT (Coralville, IA). Purification of the (8,4) nanotube chirality suspended using the $(GT)_{20}$ sequence was performed as previously described.⁵⁶

Near-Infrared Fluorescence Spectroscopy of Carbon Nanotubes in Solution. Near-infrared fluorescence emission spectra from aqueous nanotube solutions were acquired using a home-built apparatus consisting of a tunable white light laser source, inverted microscope, and InGaAs near-infrared detector. The SuperK EXTREME supercontinuum white light laser source (NKT Photonics) was used with a VARIA variable bandpass filter accessory capable of tuning the output 500-825 nm with a bandwidth of 20 nm. The light path was shaped and fed into the back of an inverted IX-71 microscope (Olympus) where it passed through a 20× near-infrared objective (Olympus) and illuminated a 50–100 μ L nanotube sample in a 96-well plate (Corning). The emission from the nanotube sample was collected through the 20× objective and passed through a dichroic mirror (875 nm cutoff, Semrock). The light was f/# matched to the spectrometer using several lenses and injected into an Isoplane spectrograph (Princeton Instruments) with a slit width of 410 μ m which dispersed the emission using an 86 g/mm grating with 950 nm blaze wavelength. The spectral range was 930-1369 nm with a resolution of ~0.7 nm. The light was collected by a NIRvana InGaAs 640 × 512 pixel array (Princeton Instruments). An HL-3-CAL-EXT halogen calibration light source (Ocean Optics) was used to correct for wavelength-dependent features in the emission intensity arising from the spectrometer, detector, and other optics. A Hg/Ne pencil style calibration lamp (Newport) was used to calibrate the spectrometer wavelength. Background subtraction was conducted using a well in a 96-well plate filled with DI H2O. Following acquisition, the data were processed with custom code written in MATLAB which applied the aforementioned spectral corrections and background subtraction and was used to fit the data with Lorentzian functions.

Solution Phase Experimental Conditions. Unless otherwise noted, the concentration of nanotubes used for all experiments was 1 mg/L. Doxorubicin hydrochloride salt (LC laboratories) was prepared in a concentrated stock solution of 5 mM in deionized water and added to samples to the indicated final concentrations. Control samples used a volume-matched addition of water. Ethidium bromide, SYBR green, and Hoechst 33258 (all from ThermoFisher) were added to a final concentration of 1 μ M. Experiments in serum used fetal

bovine serum (ThermoFisher) with concentrated nanotubes added for a negligible increase in volume. Samples were incubated for 4 h.

DNA-Displacement, Aggregation, and Doxorubicin Accumulation Measurements. DNA displacement measurements were conducted using 100 kDa Amicon centrifuge filters (Millipore) to remove displaced DNA. Absorbance of unmodified DNA was measured using the NanoDrop 2000 spectrophotometer (Thermo Fisher Scientific). DNA modified with Cy5 was measured using a Tecan Infinite M1000 plate reader (Tecan Group Ltd., Switzerland) to acquire absorbance spectra with 2 nm steps. Experiments measuring the sequestration/binding of doxorubicin to nanotubes involved a 100 μ L volume of 500 μ M doxorubicin incubated with 20 mg/L (GT)₁₅ nanotubes. The samples were then centrifuged at maximum speed (21130 RCF) for 5 min to pellet the nanotubes followed by extraction of the supernatant. Absorbance spectra of the supernatant were acquired of the 350-700 nm range, using 2 nm steps, and compared to an identically treated control sample without nanotubes. A standard curve was constructed with known concentrations of doxorubicin to calculate the mass of doxorubicin that was lost due to the presence of nanotubes. The pellet of nanotubes was then washed in an attempt to liberate bound doxorubicin, which was again assessed by the absorbance spectra of the supernatant and comparison to the standard curve. Quantification of aggregation was done using dynamic light scattering (Zetasizer Nano ZS, Malvern Instruments) for three independent runs.

Near-Infrared Hyperspectral Microscopy. Near-infrared hyperspectral microscopy was performed as previously described.⁴⁶ The sample was illuminated using a continuous wave 730 nm diode laser (output power = 2 W) via a multimode fiber. A custom beam shaping module was used to produce a top hat intensity profile with a maximum of 20% variation at the sample surface. Shaped laser emission was reflected into an Olympus IX-71 inverted microscope modified for near-infrared transmission and focused onto the sample with a 100× (UAPON100XOTIRF; numerical aperture, NA = 1.49) oil objective (Olympus) via a long-pass dichroic mirror with a cut-on wavelength of 880 nm. Spatially resolved, nearinfrared emission from the sample was fed into a volume Bragg grating (VBG) where specific wavelength components of the polychromatic light were diffracted and passed again through the VBG resulting in a monochromatic beam, which was collected by a 256 × 320 pixel InGaAs array (Photon Etc.). Data were compiled as a continuous stack of images for the indicated wavelength ranges (hyperspectral cubes) wherein every pixel of a near-infrared image was spectrally resolved.

Single-Nanotube Measurements. Single-nanotube measurements were performed by incubating (GT)₁₅-suspended nanotubes on a poly-D-lysine-coated glass bottom plate (Mattek, Ashland, MA) for 10 min before washing with 20 mM HEPES buffer three times and adding 1 mL of 20 mM HEPES buffer containing (±)-6-hydroxy-2,5,7,8-tetramethyl-chromane-2-carboxylic acid (Trolox) at 2 mg/mL. Hyperspectral cubes were obtained as described before and after addition of 50 $\mu{\rm M}$ doxorubicin. Three independent runs were performed. Data were processed with ImageJ software. Peaks were fitted to Lorentzian functions using custom MATLAB code to obtain center wavelength values, and the differences of each nanotube from each condition were pooled to make average spectra and construct box and whisker plots.

Measurement of Nanotube Response to Doxorubicin in Cells. A murine macrophage cell line (RAW 264.7, TIB-71 obtained from ATCC) was propagated at 37 °C and 5% CO₂ in DMEM with 10% heat-inactivated FBS, 2.5% HEPES, 1% glutamine, and 1% penicillin/streptomycin (all from Gibco). Cells were plated on glass bottom Petri-dishes (Mattek) and treated with 1 mg/mL (GT)₁₅ nanotubes added directly to the medium overnight. Cells were washed in warm PBS three times before treatment with buffer or 500 μM doxorubicin for 1 h, and hyperspectral measurements were performed. For both the buffer-treated and doxorubicin-treated cells, regions of interest (ROIs) were selected using ImageJ software around cells with measurable nanotube fluorescence. Spectra from nanotubes within individual cells were fitted to a Lorentzian function using custom MATLAB code to obtain center wavelength values (>0.75 R^2). Center wavelength values for nanotubes within cells were averaged and compared between buffer-treated and doxorubicin-treated groups.

Device Implantation and in Vivo Measurements. All animal experiments were approved by the Institutional Animal Care and Use Committee at Memorial Sloan Kettering Cancer Center. KrosFlo Implant Membranes (500 kDa MWCO) were obtained from Spectrum Laboratories (Rancho Dominguez, CA). The membrane was cut to about 1-2 cm in length and filled with approximately 15 μ L of 1 mg/L (GT)₁₅ nanotubes. Each end was heat-sealed. All mice used were NU/J (nude) from Jackson Laboratories and anesthetized with 2% isoflurane for surgeries and spectra acquisition. The initial assessment of responsivity in vivo used three mice with a 1 mL injection of 500 μ M doxorubicin. Dose-escalation studies used N=3-4. Kinetics after injection of doxorubicin and whole-mouse hyperspectral imaging of anatomic compartment-specific sensing is reported for one mouse each. Probe-based measurements were taken using a custom-built reflectance probe-based spectroscopy system. The system consisted of a continuous wave 1 W 730 nm diode laser (Frankfurt). The laser light was injected into a bifurcated fiber optic reflection probe bundle. The sample leg of the bundle included one 200 μ m, 0.22 NA fiber optic cable for sample excitation located in the center of six 200 μ m, 0.22 NA fiber optic cables for collection of the emitted light. Emission below 1050 nm was filtered using long-pass filters, and the light was focused into the slit of a Czerny-Turner spectrograph with 303 mm focal length (Shamrock 303i, Andor). The slit width of the spectrograph was set at 410 μ m. The light was dispersed using an 85 g/mm grating with 1350 nm blaze wavelength and collected with an iDus InGaAs camera (Andor). Spectra were fitted to Lorentzian functions using custom MATLAB code. Whole-mouse hyperspectral imaging of nanotubes in vivo was performed using a preclinical hyperspectral mouse imaging system (Photon Etc., Montreal). Two continuous wave 730 nm diode lasers each with an output power of 2 W were reflected off optical mirrors and distributed over the entire mouse, resulting in a maximum power density of 340 mW/ cm². Emission light was filtered through an 1100 nm long-pass filter to reduce autofluorescence. Intensity from broadband imaging was quantified with custom software (PhySpec, Photon Etc.). Hyperspectral cubes were obtained via a volume Bragg grating (VBG) as found in the hyperspectral microscopy of cells and single nanotubes.⁴⁶

ASSOCIATED CONTENT

S Supporting Information

The Supporting Information is available free of charge on the ACS Publications website at DOI: 10.1021/acs.nanolett.9b00956.

Additional methods and figures including sensor kinetics, representative sensor spectra, the role of aggregation and purity on sensor response, assessing DNA displacement on the sensor, measuring doxorubicin affinity for binding the sensor, the effect of washing the sensor, the lack of correlation between intracellular sensor wavelength and intensity, *in vitro* response, sensor dose response within an implantable membrane, *in vivo* sensor dose response to doxorubicin, and *in vivo* hyperspectral analysis of the implantable sensor (PDF)

AUTHOR INFORMATION

Corresponding Author

*E-mail: hellerd@mskcc.org. Phone: 646-888-3419.

ORCID ®

Jackson D. Harvey: 0000-0001-8700-0713 Ryan M. Williams: 0000-0002-2381-8732 Daniel A. Heller: 0000-0002-6866-0000

Author Contributions

J.D.H. and R.M.W. contributed equally.

Notes

The authors declare the following competing financial interest(s): D.A.H. is a cofounder and officer with equity interest in LipidSense, Inc. and Goldilocks Therapeutics, Inc. D.A.H. is a member of the scientific advisory board of Oncorus, Inc. R.M.W. is a scientific advisor with equity interest in Goldilocks Therapeutics, Inc. H.A.B. is a cofounder of Pictesque, Inc.

ACKNOWLEDGMENTS

This work was supported in part by the NIH New Innovator Award (DP2-HD075698), the Cancer Center Support Grant (P30 CA008748), the National Science Foundation CAREER Award (1752506), the American Cancer Society Research Scholar Grant (GC230452), the Pershing Square Sohn Cancer Research Alliance, the Honorable Tina Brozman Foundation for Ovarian Cancer Research, the Expect Miracles Foundation-Financial Services Against Cancer, the Anna Fuller Fund, the Louis V. Gerstner Jr. Young Investigator's Fund, the Frank A. Howard Scholars Program, Cycle for Survival, the Alan and Sandra Gerry Metastasis Research Initiative, Mr. William H. Goodwin and Mrs. Alice Goodwin and the Commonwealth Foundation for Cancer Research, the Experimental Therapeutics Center, the Imaging & Radiation Sciences Program, and the Center for Molecular Imaging and Nanotechnology of Memorial Sloan Kettering Cancer. R.M.W. was supported by the Ovarian Cancer Research Fund [Ann Schreiber Mentored Investigator Award 370463] and the American Heart Association Postdoctoral Fellowship (17POST33650043). K.M.T. was supported in part by National Cancer Institute Grant NIH T32 CA062948. H.A.B. was supported by a Medical Scientist Training Program grant from the National Institute of General Medical Sciences of the NIH under award T32GM007739 to the Weill Cornell/ Rockefeller/Sloan-Kettering Tri-Institutional MD-PhD Pro-

gram. Y.S. was supported by the Center for Metastasis Research Scholars Fellowship Program at Memorial Sloan Kettering Cancer Center. The authors would like to thank P. Jena and D. Roxbury for instrument automation and MATLAB code, as well as helpful discussions, and J. Budhathoki-Uprety for helpful discussions. All data needed to evaluate the conclusions in the paper are present in the paper and/or the Supporting Information. Additional data and code related to this paper may be requested from the authors.

REFERENCES

- (1) Katzung, B. G.; Masters, S. B.; Trevor, A. J. Basic & clinical pharmacology, 11th ed.; McGraw-Hill Medical: New York, 2009; pp xiii. 1218.
- (2) Tacar, O.; Sriamornsak, P.; Dass, C. R. Doxorubicin: an update on anticancer molecular action, toxicity and novel drug delivery systems. *J. Pharm. Pharmacol.* **2013**, *65*, 157–170.
- (3) Vonhoff, D. D.; Layard, M. W.; Basa, P.; Davis, H. L.; Vonhoff, A. L.; Rozencweig, M.; Muggia, F. M. Risk-Factors for Doxorubicin-Induced Congestive Heart-Failure. *Ann. Intern. Med.* **1979**, *91*, 710–717
- (4) Minow, R. A.; Benjamin, R. S.; Lee, E. T.; Gottlieb, J. A. Adriamycin cardiomyopathy—risk factors. *Cancer* **1977**, 39, 1397—1402
- (5) Lefrak, E. A.; Pit'ha, J.; Rosenheim, S.; Gottlieb, J. A. A clinicopathologic analysis of adriamycin cardiotoxicity. *Cancer* **1973**, 32, 302–314.
- (6) Goodman, M. D.; McPartland, S.; Detelich, D.; Saif, M. W. Chemotherapy for intraperitoneal use: a review of hyperthermic intraperitoneal chemotherapy and early post-operative intraperitoneal chemotherapy. *J. Gastrointest Oncol* **2016**, *7*, 45–57.
- (7) Rossi, C. R.; et al. Hyperthermic Intraoperative intraperitoneal chemotherapy with cisplatin and doxorubicin in patients who undergo cytoreductive surgery for peritoneal carcinomatosis and sarcomatosis Phase I study. *Cancer* **2002**, *94*, 492–499.
- (8) Cheung-Ong, K.; Giaever, G.; Nislow, C. DNA-Damaging Agents in Cancer Chemotherapy: Serendipity and Chemical Biology. *Chem. Biol.* **2013**, *20*, 648–659.
- (9) Ren, J.; Jenkins, T. C.; Chaires, J. B. Energetics of DNA intercalation reactions. *Biochemistry* **2000**, *39*, 8439–47.
- (10) Smith, S. B.; Finzi, L.; Bustamante, C. Direct Mechanical Measurements of the Elasticity of Single DNA-Molecules by Using Magnetic Beads. *Science* **1992**, *258*, 1122–1126.
- (11) Koster, D. A.; Palle, K.; Bot, E. S. M.; Bjornsti, M. A.; Dekker, N. H. Antitumour drugs impede DNA uncoiling by topoisomerase I. *Nature* **2007**, 448, 213–217.
- (12) Hurley, L. H. DNA and its associated processes as targets for cancer therapy. *Nat. Rev. Cancer* **2002**, *2*, 188–200.
- (13) Harvey, R. G.; Geacintov, N. E. Intercalation and Binding of Carcinogenic Hydrocarbon Metabolites to Nucleic-Acids. *Acc. Chem. Res.* 1988, 21, 66–73.
- (14) Lepecq, J. B.; Paoletti, C. A Fluorescent Complex between Ethidium Bromide and Nucleic Acids Physical-Chemical Characterization. *J. Mol. Biol.* **1967**, 27, 87–106.
- (15) Spence, M. T. Z.; Johnson, I. D. The molecular probes handbook: a guide to fluorescent probes and labeling technologies, 11th ed.; Live Technologies Corporation: Carlsbad, CA, 2010; pp xiv, 1160.
- (16) Martin, R. M.; Leonhardt, H.; Cardoso, M. C. DNA labeling in living cells. *Cytometry, Part A* **2005**, *67A*, 45–52.
- (17) Straif, K.; Baan, R.; Grosse, Y.; Secretan, B.; El Ghissassi, F.; Cogliano, V. Carcinogenicity of polycyclic aromatic hydrocarbons. *Lancet Oncol.* **2005**, *6*, 931–932.
- (18) Miguel, A. H.; Kirchstetter, T. W.; Harley, R. A.; Hering, S. V. On-road emissions of particulate polycyclic aromatic hydrocarbons and black carbon from gasoline and diesel vehicles. *Environ. Sci. Technol.* **1998**, 32, 450–455.

(19) Kumke, M. U.; Lohmannsroben, H. G.; Roch, T. Fluorescence spectroscopy of polynuclear aromatic compounds in environmental monitoring. *J. Fluoresc.* **1995**, *5*, 139–52.

- (20) Baughman, R. H.; Zakhidov, A. A.; de Heer, W. A. Carbon nanotubes the route toward applications. *Science* **2002**, 297, 787–792.
- (21) Zheng, M.; Jagota, A.; Semke, E. D.; Diner, B. A.; McLean, R. S.; Lustig, S. R.; Richardson, R. E.; Tassi, N. G. DNA-assisted dispersion and separation of carbon nanotubes. *Nat. Mater.* **2003**, *2*, 338–42.
- (22) Roxbury, D.; Tu, X.; Zheng, M.; Jagota, A. Recognition ability of DNA for carbon nanotubes correlates with their binding affinity. *Langmuir* **2011**, 27, 8282–93.
- (23) Manohar, S.; Tang, T.; Jagota, A. Structure of homopolymer DNA-CNT hybrids. J. Phys. Chem. C 2007, 111, 17835–17845.
- (24) O'Connell, M. J.; et al. Band gap fluorescence from individual single-walled carbon nanotubes. *Science* **2002**, 297, 593–6.
- (25) Wang, F.; Dukovic, G.; Brus, L. E.; Heinz, T. F. The optical resonances in carbon nanotubes arise from excitons. *Science* **2005**, 308, 838–41.
- (26) Cheong, W. F.; Prahl, S. A.; Welch, A. J. A review of the optical properties of biological tissues. *IEEE J. Quantum Electron.* **1990**, 26, 2166–2185.
- (27) Gao, J.; Gomulya, W.; Loi, M. A. Effect of medium dielectric constant on the physical properties of single-walled carbon nanotubes. *Chem. Phys.* **2013**, *413*, 35–38.
- (28) Choi, J. H.; Strano, M. S. Solvatochromism in single-walled carbon nanotubes. *Appl. Phys. Lett.* **2007**, *90*, 223114.
- (29) Roxbury, D.; Jena, P. V.; Shamay, Y.; Horoszko, C. P.; Heller, D. A. Cell Membrane Proteins Modulate the Carbon Nanotube Optical Bandgap via Surface Charge Accumulation. *ACS Nano* **2016**, 10, 499–506.
- (30) Jena, P. V.; et al. A carbon nanotube optical reporter maps endolysosomal lipid flux. ACS Nano 2017, 11, 10689–10703.
- (31) Heller, D. A.; Jeng, E. S.; Yeung, T. K.; Martinez, B. M.; Moll, A. E.; Gastala, J. B.; Strano, M. S. Optical detection of DNA conformational polymorphism on single-walled carbon nanotubes. *Science* **2006**, *311*, 508–11.
- (32) Barone, P. W.; Baik, S.; Heller, D. A.; Strano, M. S. Near-infrared optical sensors based on single-walled carbon nanotubes. *Nat. Mater.* **2004**, *4*, 86–92.
- (33) Harvey, J. D.; Jena, P. V.; Baker, H. A.; Zerze, G. H.; Williams, R. M.; Galassi, T. V.; Roxbury, D.; Mittal, J.; Heller, D. A. A carbon nanotube reporter of microRNA hybridization events in vivo. *Nature Biomedical Engineering* **2017**, *1*, 0041.
- (34) Harvey, J. D.; Baker, H. A.; Mercer, E.; Budhathoki-Uprety, J.; Heller, D. A. Control of Carbon Nanotube Solvatochromic Response to Chemotherapeutic Agents. *ACS Appl. Mater. Interfaces* **2017**, *9*, 37947–37953.
- (35) Del Bonis-O'Donnell, J. T.; Pinals, R.; Jeong, S.; Thakrar, A.; Wolfinger, R.; Landry, M. P. Chemometric Approaches for Developing Infrared Nanosensors to Image Anthracyclines. *Biochemistry* **2019**, *58*, 54.
- (36) Iverson, N. M.; et al. In vivo biosensing via tissue-localizable near-infrared-fluorescent single-walled carbon nanotubes. *Nat. Nanotechnol.* **2013**, *8*, 873–80.
- (37) Williams, R. M.; et al. Noninvasive ovarian cancer biomarker detection via an optical nanosensor implant. *Science advances* **2018**, *4*, No. eaaq1090.
- (38) Zhang, J.; Lee, J. K.; Wu, Y.; Murray, R. W. Photoluminescence and electronic interaction of anthracene derivatives adsorbed on sidewalls of single-walled carbon nanotubes. *Nano Lett.* **2003**, *3*, 403–407
- (39) Chen, R. J.; Zhang, Y. G.; Wang, D. W.; Dai, H. J. Noncovalent sidewall functionalization of single-walled carbon nanotubes for protein immobilization. *J. Am. Chem. Soc.* **2001**, *123*, 3838–3839.
- (40) Liu, Z.; Sun, X. M.; Nakayama-Ratchford, N.; Dai, H. J. Supramolecular chemistry on water-soluble carbon nanotubes for drug loading and delivery. *ACS Nano* **2007**, *1*, 50–56.

(41) Liu, Z.; Fan, A. C.; Rakhra, K.; Sherlock, S.; Goodwin, A.; Chen, X. Y.; Yang, Q. W.; Felsher, D. W.; Dai, H. J. Supramolecular Stacking of Doxorubicin on Carbon Nanotubes for In Vivo Cancer Therapy. *Angew. Chem., Int. Ed.* **2009**, *48*, 7668–7672.

- (42) Krischke, M.; et al. Pharmacokinetic and pharmacodynamic study of doxorubicin in children with cancer: results of a "European Pediatric Oncology Off-patents Medicines Consortium" trial. Cancer Chemother. Pharmacol. 2016, 78, 1175–1184.
- (43) Agudelo, D.; Bourassa, P.; Bruneau, J.; Berube, G.; Asselin, E.; Tajmir-Riahi, H. A. Probing the Binding Sites of Antibiotic Drugs Doxorubicin and N-(trifluoroacetyl) Doxorubicin with Human and Bovine Serum Albumins. *PLoS One* **2012**, *7*, e43814.
- (44) Roxbury, D.; Jena, P. V.; Shamay, Y.; Horoszko, C. P.; Heller, D. A. Cell Membrane Proteins Modulate the Carbon Nanotube Optical Bandgap via Surface Charge Accumulation. *ACS Nano* **2016**, 10, 499–506.
- (45) Ignatova, T.; Chandrasekar, S.; Pirbhai, M.; Jedlicka, S. S.; Rotkin, S. V. Micro-Raman spectroscopy as an enabling tool for long-term intracellular studies of nanomaterials at nanomolar concentration levels. *J. Mater. Chem. B* **2017**, *5*, 6536.
- (46) Roxbury, D.; Jena, P. V.; Williams, R. M.; Enyedi, B.; Niethammer, P.; Marcet, S.; Verhaegen, M.; Blais-Ouellette, S.; Heller, D. A. Hyperspectral Microscopy of Near-Infrared Fluorescence Enables 17-Chirality Carbon Nanotube Imaging. *Sci. Rep.* **2015**, 5, 14167.
- (47) Heller, D. A.; Baik, S.; Eurell, T. E.; Strano, M. S. Single-walled carbon nanotube spectroscopy in live cells: towards long-term labels and optical sensors. *Adv. Mater.* **2005**, *17*, 2793–2799.
- (48) Yaron, P. N.; Holt, B. D.; Short, P. A.; Lösche, M.; Islam, M. F.; Dahl, K. N. Single wall carbon nanotubes enter cells by endocytosis and not membrane penetration. *J. Nanobiotechnol.* **2011**, *9*, 45.
- (49) Cui, X.; Wan, B.; Yang, Y.; Ren, X.; Guo, L. H. Length effects on the dynamic process of cellular uptake and exocytosis of single-walled carbon nanotubes in murine macrophage cells. *Sci. Rep.* **2017**, 7, 1518.
- (50) Heller, D. A.; Baik, S.; Eurell, T. E.; Strano, M. S. Single-Walled Carbon Nanotube Spectroscopy in Live Cells: Towards Long-Term Labels and Optical Sensors. *Adv. Mater.* **2005**, *17*, 2793–2799.
- (51) Jena, P. V., et al. A Carbon Nanotube Optical Reporter Maps Endolysosomal Lipid Flux. 2017, bioRxiv:134999. bioRxiv preprint server. https://www.biorxiv.org/content/10.1101/134999v2.
- (52) Galassi, T. V.; Jena, P. V.; Roxbury, D.; Heller, D. A. Single Nanotube Spectral Imaging To Determine Molar Concentrations of Isolated Carbon Nanotube Species. *Anal. Chem.* **2017**, *89*, 1073–1077
- (53) Wang, F.; Dukovic, G.; Knoesel, E.; Brus, L. E.; Heinz, T. F. Observation of rapid Auger recombination in optically excited semiconducting carbon nanotubes. *Phys. Rev. B: Condens. Matter Mater. Phys.* **2004**, *70*, 241403R.
- (54) Larsen, B. A.; Deria, P.; Holt, J. M.; Stanton, I. N.; Heben, M. J.; Therien, M. J.; Blackburn, J. L. Effect of solvent polarity and electrophilicity on quantum yields and solvatochromic shifts of single-walled carbon nanotube photoluminescence. *J. Am. Chem. Soc.* **2012**, 134, 12485–91.
- (55) Harrison, L. E.; Bryan, M.; Pliner, L.; Saunders, T. Phase i trial of pegylated liposomal doxorubicin with hyperthermic intraperitoneal chemotherapy in patients undergoing cytoreduction for advanced intra-abdominal malignancy. *Annals of surgical oncology* **2008**, *15*, 1407–1413
- (56) Ao, G. Y.; Khripin, C. Y.; Zheng, M. DNA-Controlled Partition of Carbon Nanotubes in Polymer Aqueous Two-Phase Systems. *J. Am. Chem. Soc.* **2014**, *136*, 10383–10392.